CrystEngComm

Accepted Manuscript

ROYAL SOCIETY OF CHEMISTRY

www.rsc.org/crystengcomm

Cite this: DOI: 10.1039/c0xx00000x

www.rsc.org/xxxxxx

ARTICLE TYPE

Morphology tuning of noble metal nanoparticles by diffusion-reaction control†

Feng Ye,[a] Hui Liu,[ab] Wenlai Huang[c]* and Jun Yang[a]*

Received (in XXX, XXX) Xth XXXXXXXXX 20XX, Accepted Xth XXXXXXXXX 20XX

DOI: 10.1039/b000000x

Controlling the morphology of noble metal nanoparticles can be an effective way to produce nanomaterials with favourable properties. Herein, we report our study on the effects of diffusion rate and reaction kinetics on the morphology of a number of noble metal (Au, Ag, Pd, and Pt) nanoparticles. A glass reactor based on electrochemical reduction or photo-reduction approach has been designed to achieve the control of diffusion and chemical reduction of the different noble metal precursors. The results show that the noble metal nanoparticles with flower-like, core-shell, or wheel-like morphologies could be obtained under relatively high diffusion rate due to the presence of additional growth of metal precursors on the preformed metal nuclei, while at relatively low diffusion, the noble metal nanoparticles as-prepared are small and quasi-spherical due to the relatively fast reduction of metal precursors. The experimental observations are also confirmed qualitatively by the kinetic Monte Carlo (kMC) simulations. Since diffusion and reaction kinetics are universal and key factors in the synthesis of nanomaterials, the finding in this work might have provided an effective way to manipulate the morphology of nanomaterials for a given application.

1 Introduction

Synthesis of noble metal nanoparticles (NMNPs) with morphology control has garnered sustained research interest because the properties of particles are not only dependent on their sizes, but also on their shapes.[1,2] It has been demonstrated that in a number of cases the catalytic activity and optical property of NMNPs depend sensitively on the morphology of the particles.[3–5] For instance, compared with the spherical Pt/C catalysts, the Pt-containing nanodendrites exhibited excellent performance in catalyzing methanol oxidation at room-temperature, which is usually stemmed from the porous structure, large specific surface area, many hot catalytic spots, and high-index exposed facets in the dendritic nanoparticles.[6] Up to today, a large number of approaches have been developed for the synthesis of NMNPs with different morphologies, including wires,[7–10] rods,[8,11–14] cubes,[15–21] and prisms,[22–24] using solution chemistry methods in polar and non-polar environments. Because most specific morphologies are formed at conditions far from thermodynamic equilibrium, the kinetic parameters play an important role in shaping particles.[25] Among the kinetic factors, diffusion and reaction are two general important factors influencing the structure of materials.[26,27] Most recently, Han and co-workers studied the role of compromise between diffusion and reaction in shaping the structure of calcium carbonate particles.[28–30] They designed a reactor composed of three cells, which are separated by two movable baffles and micro membranes. The reactants (aqueous solution of calcium chloride and sodium carbonate), which are pre-placed into the two side cells, respectively, diffuse and react at the middle cell after removal of the baffles. The authors found that the microscopic processes of diffusion and reaction and their compromise have significant influence on the morphology of calcium carbonate particles produced. Unfortunately, the authors utilized the concentration to achieve the diffusion control of reactants in their designed reactor, and this leads to the difference in overall amount (masses or moles) in the final product. Therefore, the effect of the overall amount on the morphologies of final calcium carbonate particles cannot be ruled out.

In this work, we aim to study the influence of diffusion/reaction on the morphology tuning of NMNPs. A reactor based on electrochemical reduction or photo-reduction was designed to manipulate the diffusion and chemical reaction of the different noble metal precursors. In this design, the diffusion of reactants was controlled by the distance from the starting point to the reaction site, while the reaction was regulated by the intensity of electric current or light. As we will see, by controlling the diffusion and reaction kinetics, a number of NMNPs with different size/morphologies are synthesized, and the results suggest that under relative rapid diffusion state, the NMNPs thus obtained are large in size and irregular in shape, while at relative low diffusion, the NMNPs with small size and quasi-spherical shape are the dominant product. The remarkable difference in morphology of NMNPs fabricated under different diffusion/reaction conditionc was also simulated using the kinetic Monte Carlo method. This study may offer a vivid example to demonstrate the tailoring of noble metal nanoparticles by means of a process controlling, and provide a method with remarkable

simplicity for creating nanostructured noble metal materials for given technological applications.

2 Experimental

2.1 General materials

Silver nitrate (ACS reagent, ≥99.0%), gold(III) chloride trihydrate ($HAuCl_4 \cdot 3H_2O$, ≥99.9%), sodium tetrachloropalladate(II) (Na_2PdCl_4, 98%), and chloroplatinic acid hydrate (H_2PtCl_6, 99.995% trace metal basis) from Sigma-Aldrich, indium tin oxide (ITO, resistance of 28.5 Ω) from CSG Holding CO. LTD, hexadecyltrimethylammonium bromide (CTAB, 98%) from Aladdin Reagents, and ethanol (99.5%) from Beijing Chemical Works, were used as received. De-ionized water was purified by a Milli-Q water purification system. All glassware and Teflon-coated magnetic stir bars were cleaned with *aqua regia*, followed by copious rinsing with de-ionized water before drying in an oven.

2.2 Synthesis of NMNPs

A reactor was specially designed to realize the diffusion-reaction control for the synthesis of NMNPs, as shown in Fig. 1, which is a vessel consisting of a body cylinder and two ear cylinders connected each other. The diameters of the body cylinder and ear cylinder are 30 mm and 10 mm, respectively. The length from the outer surface of ear cylinder to the surface of body cylinder, labeled as "*L*" in Fig. 1, was used to control the diffusion of metal precursors, while the reaction kinetics was controlled using the density of electric current.

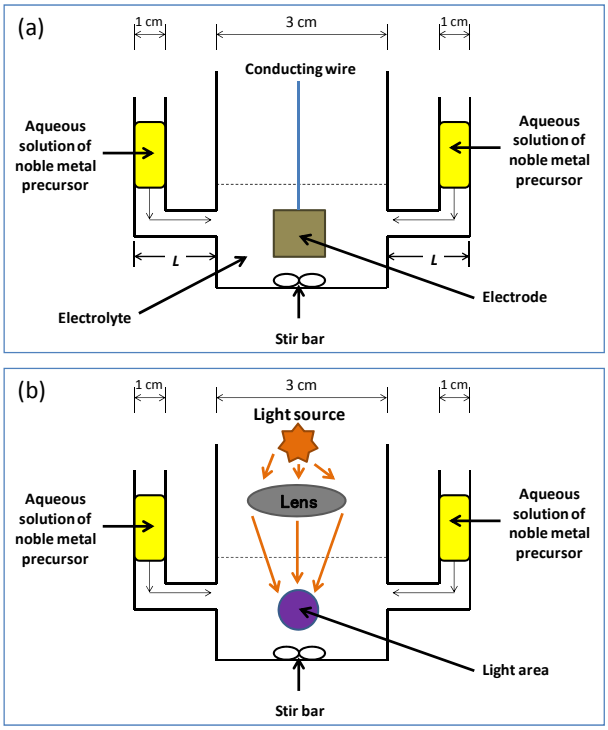

Fig. 1 A glass reactor designed to realize the diffusion-reaction control for the morphology tuning of noble metal nanoparticles using electrochemical reduction approach (a), or photo-reduction approach (b).

For the synthesis of Au nanoparticles using electrochemical reduction approach (Fig. 1a), 90 mL of 0.1 M aqueous KCl solution was added to the reactor, while 0.25 mL of aqueous $HAuCl_4$ solution (25 mM) was introduced to the two ear cylinders, respectively. An ITO slice with length and width of 10 mm was used for the deposition of Au nanoparticles through a galvanostatic deposition. The conter electrode was Pt sheet. The "*L*" of 50 mm, 100 mm, and 150 mm and the current densities of 0.1 mA/cm^2, 0.33 mA/cm^2, and 0.66 mA/Cm^2 were used to control the diffusion and reaction kinetics, respectively.

The experimental conditions for the synthesis of Pd and Pt nanoparticles were same as those for Au, besides the solution added to the ear cylinder was 0.5 mL of aqueous Na_2PdCl_4 solution and aqueous H_2PtCl_6 solution with concentration of 10 mM. For the electrochemical synthesis of Ag nanoparticles, the KCl electrolyte was replaced with aqueous $NaNO_3$ solution (0.1 M) to avoid the formation of AgCl precipitates, while other conditions were kept same as those for the synthesis of Au nanoparticles.

The reduction of noble metal precursors could also be induced by light. As shown in Fig. 1b, the light irradiated from a 300 W Xenon lamp was concentrated into a spot in the solution through a convergent lens. 0.5 mmol of CTAB and a small amount of ethanol were added as stabiling agent and sacrificial agent, respectively. The noble metal ions diffused into this spot area would be reduced into metal atoms, followed by nucleation and growth to form nanoparticles.

2.3 Particle characterizations

Scanning electron microscopy (SEM) was carried out on a JSM-7100F operated at a beam energy of 10 kV. Transmission electron microscopy (TEM) was performed on a JEOL JEM-2100 electron microscope operated at 200 kV with a supplied software for automated electron tomography. For the TEM measurements, a drop of the nanoparticle solution was dispensed onto a 3-mm carbon-coated copper grid. Excessive solution was removed by an absorbent paper, and the sample was dried under vacuum at room temperature. X-ray photoelectron spectroscopy (XPS) was conducted on a VG ESCALAB MKII spectrometer. Powder X-ray diffraction (XRD) patterns were recorded on a Rigaku D/Max-3B diffractometer, using Cu Kα radiation (λ = 1.54056 Å). Samples for XPS and XRD analyses were collected from the aqueous solution of nanoparticles using centrifugation, washed with ethanol several times, and then dried at room temperature in vacuum.

3 Results and discussion

In the strategy developed in this work, the diffusion and reduction reaction control of the metal precursors is an important step for the morphology tuning of NMNPs. The diffusion of metal precursors could be qualitatively controlled by the length indicated in Fig. 1. With the decrease in distance from the staring point to the reaction site, the diffusion rate of the metal precursors increases. While for the reation kinetics, it could be regulated by changing the density of electric current. The reduction of noble metal precursors at ITO electrode would be different with the change of current density. At high current density, metal precursors would be reudced quickly on the ITO electrode, and

vice versa.

3.1 Diffusion-reaction control by electrochemical reduction approach for the fabrication of NMNPs

For the electrochemical reduction approach, when the current density was fixed at 0.1 mA/cm^2, the SEM images of the NMNPs (Au, Ag, Pd, and Pt) as-prepared under L of 15 cm, 10 cm, and 5 cm were shown in Fig. 2. As indicated, with the increase of diffusion rate, the size and morphology of NMNPs were remarkably different. For Au, at low diffusion rate (L = 15 cm), the majority of final products were quasi-spherical particles with average size of ca. 149.3 nm, accompanied by a minor fraction of

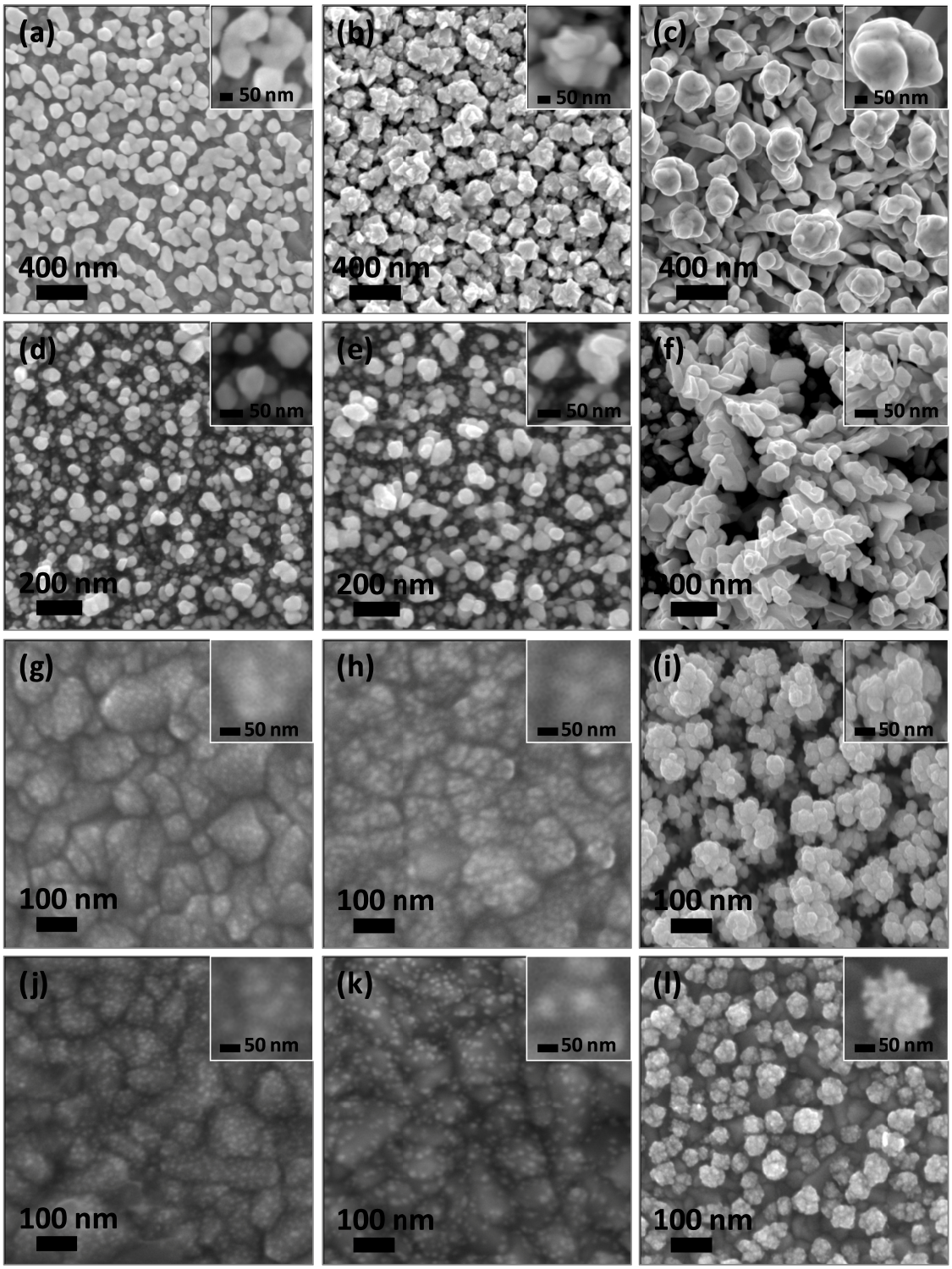

Fig. 2 SEM images of Au (a,b,c), Ag (d,e,f), Pd (g,h,i), and Pt nanoparticles (j,k,l) as-prepared using electrochemical reduction approach with the current density of 0.1 mA/cm^2 and diffusion distance (L) of 15 cm (a,d,g,j), 10 cm (b,e,h,k), and 5 cm (c,f,i,l), respectively. The inserts are the SEM images with high magnification.

worm-like particles (Fig. 2a). With the increase of diffusion rate (L = 10 cm), the morphology of Au evolved from quasi-spherical particles to flower-like aggregates, which have the average size of ca. 266.7 nm (Fig. 2b). The flower-like aggregates were composed of a number of smaller particles, as evinced by the insert in Fig. 2b. Under the highest diffusion rate in this work (L = 5 cm), the surface of the flower-like aggregates became smoother, and the long stems connected with the flower-like particles were observed (Fig. 2c). For the other three noble metal systems (Ag, Pd, and Pt), the evolution of the size/morphology of the NMNPs exhibited same trends as that for Au. At low diffusion rate (L = 15 cm and 10 cm), the NMNPs had quasi-spherical morphology and small size, while at high diffusion rate (L = 5 cm), they were dominated by flower-like particle aggregates with much big sizes. Although the surface conditions of the electrode might have influence on the formation of nuclei, the differences in particle morphology are mainly induced by different diffusion rate since the electrode remains same for all experiments.

We took the NMNPs prepared using electrochemical reduction with current density of 0.1 mA/cm^2 and L of 5 cm, respectively, as typical examples to illustrate the the crystalline nature of the final products. As shown in Fig. S1 of Electronic Supplementary Information (ESI), the XRD patterns demonstrated the successful syntheses of face-centred cubic (fcc) Au, Ag, Pd, and Pt nanoparticles.[31]

In case of diffusion length (L) fixed at 5 cm, the current density has also significant influence on the size/morphology of the noble metal nanoparticles as-prepared using electrochemical reduction approach. As a typical example, the Au nanoparticles prepared at current density of 0.33 mA/cm^2 and 0.66 mA/cm^2 were characterized by the SEM images in ESI Fig. S2. In comparison with flower-like particles obtained at current density of 0.1 mA/cm^2 (Fig. 1c), the Au products at high current densities were dominated by quasi-spherical sparticles with much smaller sizes (ca. 131.5 nm at 0.33 mA/cm^2 and ca. 65.8 nm at 0.66 mA/cm^2, respectively).

3.2 Mechanism using diffusion-reaction control for the morphology tuning of NMNPs

The mechanism for the morphology tuning of NMNPs *via* an electrochemical reduction approach could be elucidated using the scheme in Fig. 3. In colloidal chemistry method, the growth of particles might be regulated by diffusion rate and reduction kinetics.[28] Both the diffusion rate and the reaction kinetics can be the rate determining step for the particle formation. In this work, at relatively high diffusion rate, which corresponds to the short diffusion length (L), a large number of noble metal precursors diffuse to the reaction site (ITO electrode) in short time, which could not be reduced simutaneously. Only a portion of the metal ions are reduced to be metal atoms for the formation of nuclei. The excessive noble metal ions and the ions diffused continuously to the electrode would be reduced subsequently and lead to additional growth on the previously formed noble metal nuclei until the complete consumption of the precursors. Whether the nuclei grow by the so-called 'oriented attachment' mechanism[32–34] or by a continuous 'atom by atom' growth[35] after the nucleation step, such conditions appear to favor the anisotropic growth, which leads to form NMNPs with flower-like morphology. In contrast, at relative low diffusion rate, which corresponds to the long diffusion length (L) or high current density, the noble metal precursors diffused from the starting point to the reaction site are immediately reduced on the electrode to form metal nuclei. Then the metal ions subsequently diffused to the electrode are either reduced to form new nuclei at a random site on the electrode, or grow on the surface of the preformed metal nuclei, resulting in the formation of quasi-spherical particles with broad size distribution. The findings in this work were not at odds with the previously reported result on branching Zn nanoparticles prepared by diffusion-limited aggregate in a electrochemical deposition mode.[36,37] The difference suggests that the morphologies of nanoparticles grown under diffusion-controlled conditions are highly sensitive to the environment of the crystal growth. The applied voltage, the surface conditions of electrode, and the electrolyte might also play important roles in determining the final morphology of the nanoparticles. A reasonable design is therefore of necessity to investigate the influence of diffusion/reaction kinetics on the morphology of nanoparticles.

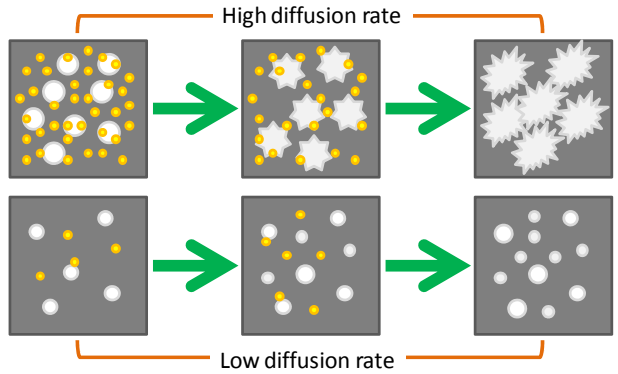

Fig. 3 Schematic to illustrate the morphology tuning of NMNPs using diffusion-reaction control by an electrochemical reduction approach. The additional growth on previously formed nuclei at high diffusion rate accounts for the formation of flower-like noble metal particles, while low diffusion rate results in the formation of nanospheres.

3.3 Diffusion-reaction control by photo-reduction approach for the fabrication of NMNPs

To eliminate the influence from the electrode on the morphology of the final NMNPs, a photo-reduction approach instead of electrochemical reduction was used to reduce the metal precursors diffused from the starting point to the reaction site, as shown in Fig. 1b. We will use Au and Ag nanosystem as typical examples to illustrate the morphology of NMNPs formed by this photo-reduction approach.

Analogous to that obtained by electrochemical reduction, the morphology of the Au nanoparticles prepared by photo-reduction approach at different diffusion length (L) was also remarkably different. As indicated by the TEM images in Fig. 4, quasi-sperical Au nanoparticles with average size of ca. 45.8 nm were obtained at diffusion length of 15 cm, which corresponds to relatively low diffusion rate. With the decrease of the diffusion

length (L), which means the increase of diffusion rate of metal precursors, Au nanoparticles with core-shell-like structure (L = 10 cm) and wheel-like structure (L = 5 cm) were the dominant products instead. The formation of core-shell or wheel-like nanostructures could also be attributed to the additional growth of Au precursors on the preformed Au nuclei due to the relatively high diffusion rate. Of course, the influence of CTAB, the stabilizing agent, on the morphology of the final Au products cannot be ruled out. It may have some contribution to the anisotropic growth of Au precursors on the surface of preformed Au nuclei.

The TEM images of Ag nanoparticles prepared by photo-reduction approach at different diffusion length (L) were demonstrated in ESI Fig. S3, which displayed similar nanostructures as those of Au. At low diffusion rate, quasi-spherical Ag nanoparticles were obtained (ESI Fig. S3a and b), while at high diffusion rate, Ag particles with complicated structures (wheel-like or dendritic) were clearly observed (ESI Fig. S3c and d).

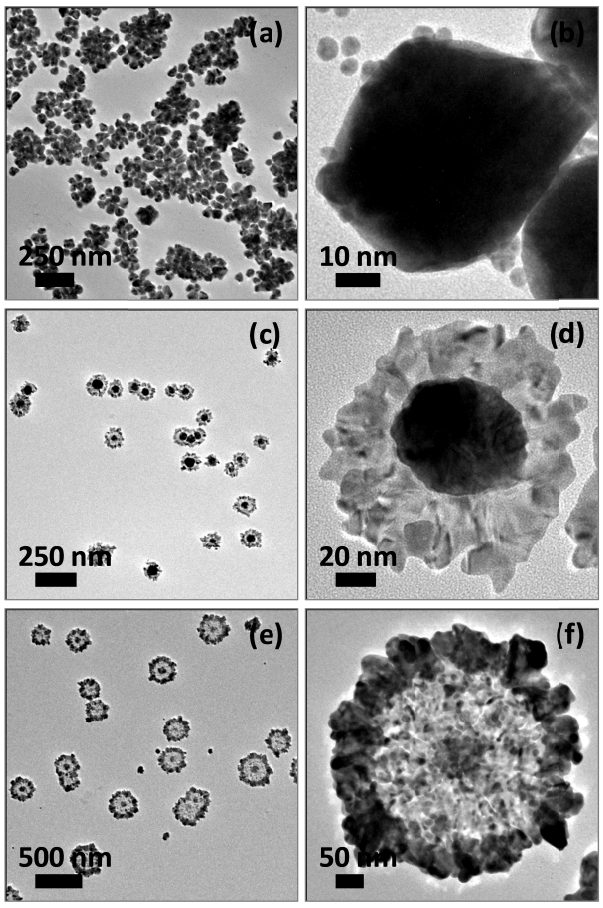

Fig. 4 TEM images with low magnification (a,c,e) and high magnification (b,d,f) of Au nanoparticles as-prepared using photo-reduction approach with the diffusion distance (L) of 15 cm (a,b), 10 cm (c,d), and 5 cm (e,f), respectively.

The surface chemistry of the Au and Ag nanoparticles prepared by photo-reduction at diffusion length (L) of 5 cm were recovered from aqueous solution by centrifugation and were subjected to XPS analysis. As shown in ESI Fig. S4, one doublet at 84.4 eV and 88.1 eV for Au 4f region ($4f_{7/2}$ and $4f_{5/2}$, respectively) and one doublet at 367.8 eV and 373.8 eV for Ag 3d region ($3d_{5/2}$ and $3d_{3/2}$, respectively), which reflect the Au and Ag at zero valent state,[38] can fit for the XPS spectra very well, indicating that the oxidation state in CTAB-stabilized Au and Ag nanoparticles prepared in this study could be neglected.

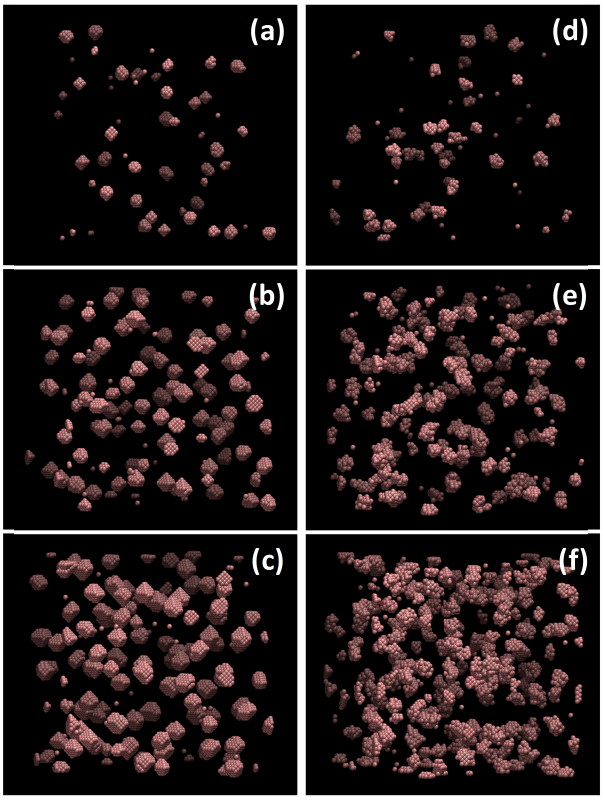

Fig. 5 The results of kMC simulations after 1×10^4 steps with the feed rate of 0.1 (a, d), 0.5 (b, e), and 1.0 (c, f). The barrier for surface diffusion is 0.0 (a, b, c) and 2.5 (d, e, f).

3.4 Simulations

To further elucidate the mechanism, we also conducted kinetic Monte Carlo (kMC) simulations for such systems. We adopted 50×50×50 fcc lattice with the site energy values from,[39] i.e., the site energy $E_i = -0.8i$, i = 1, …, 12, means the coordination number. Fig. 5 presents the snapshots after 1×10^4 steps of simulation, which reveal the influence of the feed rate, i.e., the previously mentioned diffusion rate in experiments. Here the temperature T is set to let $k_BT = 0.3$, where k_B is the Boltzmann constant. For Fig. 5a, b, and c, the feed rates are 0.1, 0.5, and 1.0, respectively. The feeding is assumed to be random in the simulation domain, and the diffusion barrier in the bulk (from one site with i = 0 to another site of i = 0) is assumed to be zero. The barriers for both reaction and surface diffusion in Fig. 5a, b, and c are also set as zero. It is observed that a higher feed rate leads to a larger particle size. This is consistent with the preceding experimental results. In Fig. 5d, e, and f, we also adopted the feed rate of 0.1, 0.5, and 1.0, respectively, but enhanced the barrier of

surface diffusion to 2.5. Besides the same trends in particle size as those in Fig. 5a~c, the particles also seem more irregular with the increase in the feed rate, agreeing with the experiments in this work we allowed only atomic diffusion, and no particle aggregation.

The influence of the reaction rate on the particle size is more obvious with a large feed rate at a higher temperature. Fig. 6 shows the snapshots after 1×10^4 steps of simulation at the temperature with k_BT = 1.2, and the feed rate is 1.0. The barrier for surface diffusion is set to be 0.7, but the reaction barrier is set to be 1.5 and 0.0 for Fig. 6a and b, respectively. The results confirm that a higher reaction rate corresponds to a smaller particle size, probably due to a higher nucleation rate.

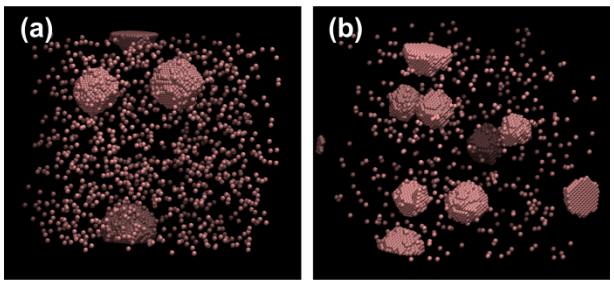

Fig. 6 The results of kMC simulations after 1×10^4 steps with the reaction barrier of 1.5 (a) and 0.0 (b).

4 Conclusions

In summary, the effects of diffusion rate and reaction kinetics on the morphology of a number of noble metal (Au, Ag, Pd, and Pt) nanoparticles were studied in this work. A glass reactor based on electrochemical reduction or photo-reduction was designed to manipulate the diffusion and chemical reduction of the different noble metal precursors. The results demonstrated that the noble metal nanoparticles with complicated morphology could be obtained under relatively high diffusion rate, while at relatively low diffusion, the noble metal nanoparticles as-prepared were small and quasi-spherical. A reasonable mechanism was proposed and simulated upon kinetic Monte Carlo method to interpret the remarkable difference in morphology of noble metal nanoparticles fabricated under different diffusion/reaction conditions. At relatively high diffusion rate, the additional growth of metal precursors on the surface of metal nuclei accounts for the formation of noble metal nanoparticles with flower-like, core-shell, or wheel-like morphologies. In contrast, at relative low diffusion rate, the noble metal precursors diffused from the starting point to the reaction site are either reduced fastly to form new nuclei at a random site of reaction area, or grow on the surface of the preformed metal nuclei, resulting in the formation of noble metal nanoparticles with quasi-spherical shape and broad size distribution.

Aknowledgement

Financial supports from State Key Laboratory of Multiphase Complex Systems, Institute of Process Engineering, Chinese Academy of Sciences (MPCS-2012-A-11), the 100 Talents Program of the Chinese Academy of Sciences, and National Natural Science Foundation of China (No.: 21173226, 21376247) is gratefully acknowledged.

Notes and references

[a] *State Key Laboratory of Multiphase Complex Systems, Institute of Process Engineering, Chinese Academy of Sciences, Beijing, China 100190. Fax: 86-10-8254 4814; Tel: 86-10-8254 4915; E-mail: jyang@ipe.ac.cn*

[b] *University of Chinese Academy of Sciences, No. 19A Yuquan Road, Beijing, China 100049*

[c] *EMMS Group, State Key Laboratory of Multiphase Complex Systems, Institute of Process Engineering, Chinese Academy of Sciences, Beijing, China 100190. Fax: 86-10-6255 8065; Tel: 86-10-8254 4942; E-mail: wlhuang@ipe.ac.cn*

†Electronic Supplementary Information (ESI) available: XRD patterns, XPS spectra, additional SEM and TEM images for the characterization of the nanostructures in this study. See DOI:10.1039/b000000x/

1. M. A. El-Sayed, *Acc. Chem. Res.*, 2001, **34**, 257.
2. Y. Xia, Y. Xiong, B. Lim and S. E. Skrabalak, *Angew. Chem. Int. Ed.*, 2009, **48**, 60.
3. J. Yang, J. Y. Lee, L. X. Chen and H.-P. Too, *J. Phys. Chem. B*, 2005, **109**, 5468.
4. Z. Peng and H. Yang, *J. Am. Chem. Soc.*, 2009, **131**, 7542.
5. B. Lim, M. Jiang, P. H. C. Camargo, E. C. Cho, J. Tao, X. Lu, Y. Zhu and Y. Xia, *Science*, 2009, **324**, 1302.
6. Y. Feng, X. Ma, L. Han, Z. Peng and J. Yang, *Nanoscale*, 2014, DOI: 10.1039/C4NR00421C.
7. K.-M. Chi and P.-Y. Chen, *J. Nanosci. Nanotechnol.*, 2008, **8**, 3379.
8. C. Wang, Y. Hou, J. Kim and S. Sun, *Angew. Chem. Int. Ed.*, 2007, **46**, 6333.
9. C. Mao, D. J. Solis, B. D. Reiss, S. T. Kottmann, R. Y. Sweeney, A. Hayhurst, G. Georgiou, B. Iverson and A. M. Belcher, *Science*, 2004, **303**, 213.
10. K. K. Caswell, C. M. Bender and C. J. Murphy, *Nano Lett.*, 2003, **3**, 667.
11. B. P. Khanal and E. R. Zubarev, *Angew. Chem. Int. Ed.*, 2009, **48**, 6888.
12. C. G. Wilson, P. N. Sisco, E. C. Goldsmith and C. J. Murphy, *J. Mater. Chem.*, 2009, **19**, 6332.
13. D. Seo, C. I. Yoo, J. Jung and H. Song, *J. Am. Chem. Soc.*, 2008, **130**, 2940.
14. F. Kim, J. H. Song and P. Yang, *J. Am. Chem. Soc.*, 2002, **124**, 14316.
15. X. Huang, H. Zhang, C. Guo, Z. Zhou and N. Zheng, *Angew. Chem. Int. Ed.*, 2009, **48**, 4808.
16. D. Kim, N. Lee, M. Park, B. H. Kim, K. An and T. Hyeon, *J. Am. Chem. Soc.*, 2009, **131**, 454.
17. L. Au, Y. Chen, F. Zhou, P. H. C. Camargo, B. Lim, Z.-Y. Li, D. S. Ginger and Y. Xia, *Nano Res.*, 2008, **1**, 441.
18. Y. Zhang, M. E. Grass, J. N. Kuhn, F. Tao, S. E. Habas, W. Huang, P. Yang and G. A. Somorjai, *J. Am. Chem. Soc.*, 2008, **130**, 5868.
19. C. Wang, H. Daimon, Y. Lee, J. Kim and S. Sun, *J. Am. Chem. Soc.*, 2007, **129**, 6974.
20. S. H. Im, Y. T. Lee, B. Wiley and Y. Xia, *Angew. Chem. Int. Ed.*, 2005, **44**, 2154.
21. Y. Sun and Y. Xia, *Science*, 2002, **298**, 2176.
22. S. S. Shankar, A. Rai, B. Ankamwar, A. Singh, A. Ahmad and M. Sastry, *Nat. Mater.*, 2004, **3**, 482.
23. R. Jin, Y. Cao, C. A. Mirkin, K. L. Kelly, G. C. Schatz and J. G. Zheng, *Science*, 2001, **294**, 1901.
24. J. Yang, Q. Zhang, J. Y. Lee and H.-P. Too, *J. Colloid Interface Sci.*, 2007, **308**, 157.
25. S. M. Lee, S. N. Cho and J. Cheon, *Adv. Mater.*, 2003, **15**, 441.
26. C. Y. Tai, M. C. Chang, C. K. Wu and Y. C. Lin, *Chem. Eng. Sci.*, 2006, **61**, 5346.
27. C. Y. Tai, *J. Chem. Eng. Jpn.*, 1997, **30**, 373.
28. H. Wang, W. Huang and Y. Han, *Particuology*, 2013, **11**, 301.
29. H. Wang, Y. Han and J. Li, *Cryst. Growth Des.*, 2013, **13**, 1820.
30. H. Wang and Y. Han, *CrystEngComm*, 2014, **16**, 1971.

31. W. F. McClune, *Powder Diffraction File Alphabetical Index Inorganic Phase*, JCPDS, Swarthmore, PA, 1980.
32. Q. Zhang, S.-J. Liu and S.-H. Yu, *J. Mater. Chem.*, 2009, **19**, 191.
33. D. Li, M. H. Nielsen, J. R. I. Lee, C. Frandsen, J. F. Banfield and J. J. De Yoreo, *Science*, 2012, **336**, 1014.
34. X. Xue, R. L. Penn, E. R. Leite, F. Huang and Z. Lin, *CrystEngComm*, 2014, **16**, 1568.
35. A. R. Tao, S. Habas and P. Yang, *Small*, 2008, **4**, 310.
36. H. Imai, *Top. Curr. Chem.*, 2007, **270**, 43.
37. T. R. Ní Mhíocháin and J. M. D. Coey, Phys. Rev. E, 2004, **69**, 061404.
38. C. D. Wagner, A. V. Naumkin, A. Kraut-Vass, J. W. Allison, C. J. Powell and J. R. Rumble, *NIST Standard Reference Database 20*, Version 3.2 (Web Version).
39. C. Wang, W. Tian, Y. Ding, Y.-Q. Ma, Z. L. Wang, N. M. Markovic, V. R. Stamenkovic, H. Daimon and S. Sun, *J. Am. Chem. Soc.*, 2010, **132**, 6524.

Graphical abstract

Morphology tuning of noble metal nanoparticles by diffusion-reaction control

Feng Ye,[a] Hui Liu,[ab] Wenlai Huang[c]* and Jun Yang[a]*

A strategy based on diffusion-reaction control was demonstrated for the morphology tuning of noble metal nanoparticles.